ISSN 0915-633X

NATIONAL INSTITUTE FOR FUSION SCIENCE

Zero-absolute-vorticity State in a Rotating Turbulent Shear Flow

M. Tanaka, S Kida, S. Yanase and G. Kawahara

(Received - Dec. 22, 1999)

NIFS-623 Jan. 2000

RESEARCH REPORT
NIFS Series

NAGOYA, JAPAN

Zero-absolute-vorticity state in a rotating turbulent shear flow

M. Tanaka[*1], S. Kida[*2], S. Yanase[*3] and G. Kawahara[*4]

[*1] *Kyoto Institute of Technology*
[*2] *National Institute for Fusion Science*
[*3] *Okayama University*
[*4] *Ehime University*

Abstract

Stability characteristics of a rotating simple shear flow modulated periodically in the shear direction is investigated by direct numerical simulation. The temporal evolution and the final profile of the mean flow are examined, starting with a random perturbation imposed on it under the assumption that the velocity and pressure fields are uniform in the mean flow direction. It is found that the mean velocity profile changes due to the shear-Coriolis instability. If there is a locally unstable region in a stable rotating simple shear, the mean velocity profile there is deformed into a linear one with nearly-zero absolute vorticity. An analogy holds between rotating uniformly sheared turbulence and thermally convective turbulence that the region of nearly-zero absolute vorticity in the former corresponds to that of nearly-uniform temperature in the latter.

Keywords: zero absolute vorticity, shear-Coriolis instability, analogy with convective turbulence

[1] Introduction

Rotating shear flows are encountered not only as a variety of natural phenomena in meteorology and astronomy, but also in engineering applications such as flows in turbomachinary. Turbulence in rotating flows exhibits distinguished features: Two-dimensionalization of flow structures along the axis of rotation and strong dependence of the flow characteristics on the amplitude and the sense of rotation relative to the mean shear vorticity. In the case of weak rotation anti-parallel to the mean shear vorticity, three-dimensional disturbances grow rapidly, whereas they decay in the case of strong rotation both parallel or anti-parallel to the mean shear vorticity. We refer to the system where the mean shear vorticity is parallel (or anti-parallel) to the rotating axis as cyclonic system (or anti-cyclonic system).

In a turbulent channel flow, turbulence characteristics are different according as the shear vorticity near the wall is parallel (at suction side) or anti-parallel (at pressure side) to the rotating axis. The mean velocity profile is then asymmetric with respect to the center of the channel. It is observed experimentally[1,2] and by the use of direct numerical simulation[3,4] that a linear mean velocity profile with nearly-zero absolute mean vorticity appears in the core region of a turbulent channel flow when the rotation rate is large. Here, the term of absolute vorticity is used for the vorticity relative to the stationary coordinate system, that is the sum of vorticity associated with the fluid motion relative to the rotating system and with the rotation of the system itself. It is found numerically[4] that the region of zero absolute mean vorticity is full of coherent structures which are similar to the longitudinal vortex tubes observed in rotating uniformly sheared turbulence with zero absolute mean vorticity[5,6]. Disappearance of absolute vorticity is also seen in other types of flows such as a rotating turbulent free-shear layer[7] and a rotating turbulent plane Couette flow[8]. However, the formation mechanism of the region of zero absolute vorticity has not been clarified yet. In this paper, we examine the temporal evolution of the mean velocity in a uni-directional turbulent shear flow which varies periodically in the shear direction in order to reveal the formation mechanism of zero absolute vorticity. This is one of the simplest non-trivial flows for understanding of the mechanism. Formulation of the problem is described in Sec. II. Numerical results of the temporal evolution of the flow are given in Sec. III. An analogy between convective turbulence and rotating shear flow turbulence is discussed in Sec. IV. Section V is devoted to concluding remarks.

[2] Formulation

2.1 Basic equations

We consider the motion of an incompressible viscous fluid in a rotating frame. In the case that a simple shear flow, $\boldsymbol{U} = (Sx_2, 0, 0)$, is rotating around the x_3-axis

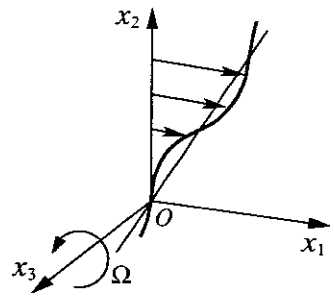

Fig. 1 Configuration.

(Fig. 1), the temporal evolution of the velocity fluctuation u_i in the rotating frame is described by

$$\frac{\partial u_i}{\partial t} + Sx_2\frac{\partial u_i}{\partial x_1} + u_k\frac{\partial u_i}{\partial x_k} = -Su_2\delta_{i1} + f\epsilon_{ij3}u_j - \frac{\partial p}{\partial x_i} + \nu\frac{\partial^2 u_i}{\partial x_k \partial x_k} \quad (1)$$

supplemented with the solenoidal condition ($\partial u_i/\partial x_i = 0$). Here, p is the pressure, ν is the kinematic viscosity of the fluid, and $f = 2\Omega$ is the Coriolis parameter, Ω being the angular velocity of the rotation. The constant fluid density ρ is set at unity. Summation convention is used for repeated subscripts. We note that the absolute vorticity of the mean shear is $(f - S)\widehat{x}_3$. Hereafter, the x_1-, x_2- and x_3-directions are called the streamwise, vertical and spanwise directions, respectively.

Turbulent shear flows are generally dominated by the longitudinal vortex tubes which almost align with the streamwise direction, and the variation of disturbances is relatively small in the x_1-direction. Hence, we consider as the first step the velocity and pressure fluctuations which are uniform in the streamwise direction and which obey

$$\frac{\partial u_1}{\partial t} + \left(u_2\frac{\partial}{\partial x_2} + u_3\frac{\partial}{\partial x_3}\right)u_1 = (f - S)u_2 + \nu\left(\frac{\partial^2}{\partial x_2^2} + \frac{\partial^2}{\partial x_3^2}\right)u_1, \quad (2a)$$

$$\frac{\partial u_2}{\partial t} + \left(u_2\frac{\partial}{\partial x_2} + u_3\frac{\partial}{\partial x_3}\right)u_2 = -\frac{\partial p}{\partial x_2} - fu_1 + \nu\left(\frac{\partial^2}{\partial x_2^2} + \frac{\partial^2}{\partial x_3^2}\right)u_2, \quad (2b)$$

$$\frac{\partial u_3}{\partial t} + \left(u_2\frac{\partial}{\partial x_2} + u_3\frac{\partial}{\partial x_3}\right)u_3 = -\frac{\partial p}{\partial x_3} + \nu\left(\frac{\partial^2}{\partial x_2^2} + \frac{\partial^2}{\partial x_3^2}\right)u_3. \quad (2c)$$

The cross-stream flow described by (2b) and (2c) is different from homogeneous and isotropic two-dimensional turbulence by the Coriolis effect ($-fu_1$) that the streamwise component of velocity influences the perpendicular components. The velocity fluctuation $\boldsymbol{u}(\boldsymbol{x};t)$ is further split into the mean $\overline{\boldsymbol{u}}(x_2;t)$ which is the spanwise average of $\boldsymbol{u}(\boldsymbol{x};t)$ and the deviation $\boldsymbol{u}'(\boldsymbol{x};t)$ from it. The subsequent evolution of the mean velocity $Sx_2+\overline{u}_1(x_2;t)$ will be investigated in the following sections.

2.2 Shear-Coriolis instability

For a later analysis the linear stability characteristics of a rotating simple shear flow is reviewed briefly. Bradshaw[9] introduced a non-dimensional parameter,

$$B = \frac{f(f-S)}{S^2} = \frac{1+Ro}{Ro^2} \quad (3)$$

and reached the conclusion, on the basis of an analogy between rotating turbulence and stratified turbulence, that the rotation stabilizes or destabilizes the simple shear flow according as B is positive or negative. Here, the parameter,

$$Ro = -\frac{S}{f}, \quad (4)$$

represents strength of the simple shear relative to the rotation and is referred to as the Rossby number. Note that $Ro = -1$ when the absolute mean vorticity is zero. According to this criterion, anti-cyclonic flows with weak rotation ($Ro < -1$) are unstable, whereas cyclonic ($Ro > 0$) or anti-cyclonic flows with strong rotation ($0 > Ro > -1$), or shearless flows ($Ro = 0$) are stable. The case of no rotation ($Ro = \infty$) or zero absolute vorticity ($Ro = -1$) is neutrally stable.

This stability criterion may be derived from the linearized equation of (2) under the assumption that the flow is uniform in the x_1-direction[10,11,12]. By neglecting viscosity, we find that a disturbance of sinusoidal-wave type, $\boldsymbol{u}(\boldsymbol{x},t) = \widetilde{\boldsymbol{u}}(\boldsymbol{k},t)e^{i\boldsymbol{k}\cdot\boldsymbol{x}}$ and $p(\boldsymbol{x},t) = \widetilde{p}(\boldsymbol{k},t)e^{i\boldsymbol{k}\cdot\boldsymbol{x}}$, obeys

$$\frac{d\widetilde{u}_1}{dt} = (-S+f)\widetilde{u}_2, \quad \frac{d\widetilde{u}_2}{dt} = -\frac{{k_3}^2}{{k_2}^2+{k_3}^2}f\widetilde{u}_1,$$

$$\widetilde{u}_3 = -\frac{k_2}{k_3}\widetilde{u}_2, \quad \widetilde{p} = \frac{ik_2}{|\boldsymbol{k}|^2}f\widetilde{u}_1, \quad (5)$$

where $\boldsymbol{k} = (0, k_2, k_3)$ is the wavenumber vector. Note that the disturbance is pressureless[12] if $k_2 = 0$. It is seen from the first two equations that the velocity field grows exponentially or oscillates in time according as $B < 0$ or > 0. We should keep in mind that Bradshaw's criterion is applied to the *linear* stability of a simple shear flow against disturbances which are uniform in the x_1-direction.

In the present study the slope of the mean velocity $Sx_2 + \overline{u}_1(x_2;t)$ varies in the x_2-direction. Hence, we introduce the *local* Rossby number of

$$Ro^{(l)}(x_2;t) = -\frac{S + d\overline{u}_1(x_2;t)/dx_2}{f}, \quad (6)$$

which may serve as an indicator of the local stability characteristics of the flow.

Table I Dependence on Rossby number

run	f	instability of rotating simple shear			unstable region
run1	2.0	stable	anti-cyclonic	$Ro = -0.5$	– – –
run2	1.5	stable	anti-cyclonic	$Ro = -0.67$	$2\pi/3 < x_2 < 4\pi/3$
run3	1	neutral	anti-cyclonic	$Ro = -1.0$	$\pi/2 < x_2 < 3\pi/2$
run4	0.5	unstable	anti-cyclonic	$Ro = -2.0$	$\pi/3 < x_2 < 5\pi/3$
run5	0	neutral	non-rotating	$Ro = \infty$	– – –
run6	−0.5	stable	cyclonic	$Ro = 2.0$	– – –

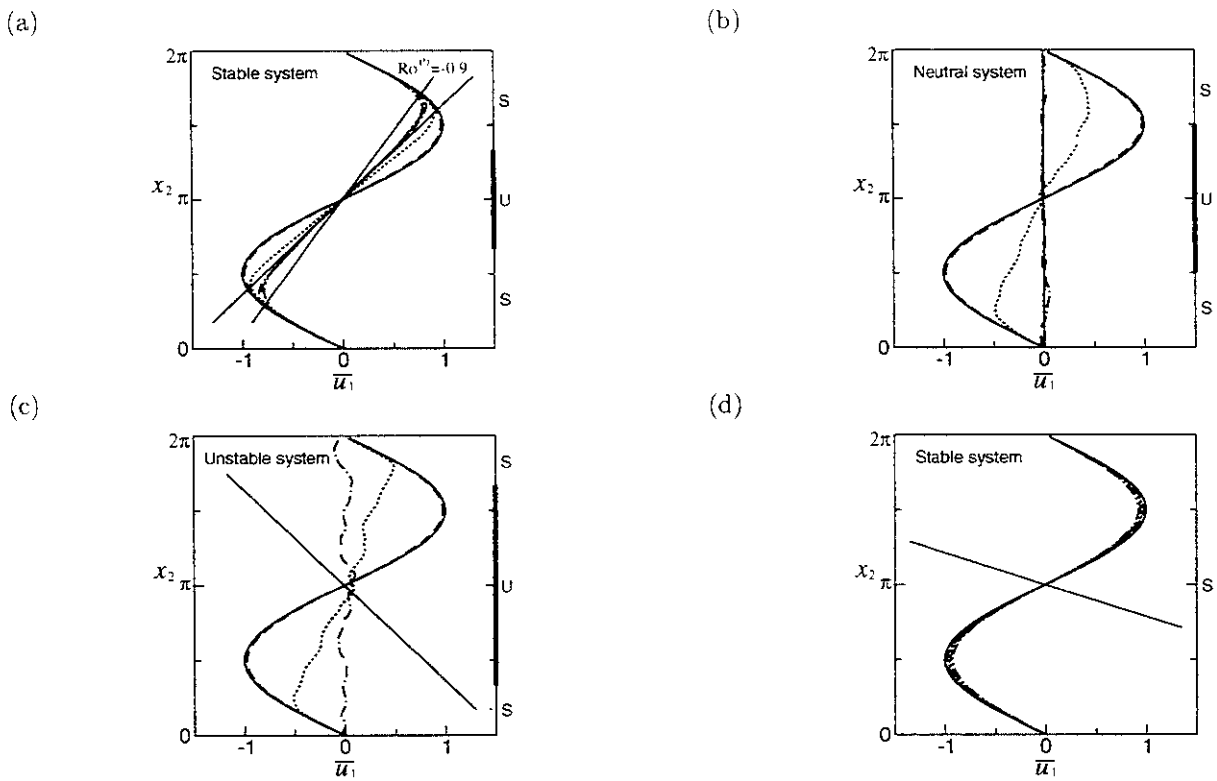

Fig. 2 Temporal evolution of mean velocity profile subtracted the simple shear component for (a) run2, (b) run3, (c) run4, and (d) run6. — ; $St = 0$, – –; $St = 5$, $\cdots$, $St = 10$, – – – ; $St = 15$, – $\cdots$ – ; $St = 20$, – $\cdots$ – ; $St = 25$. Straight lines in the figures represent the state of zero absolute vorticity ($Ro^{(l)} = -1$). The steeper line in (a) denotes $Ro^{(l)} = -0.9$.

2.3 Numerical method

Equations (2) are solved numerically using the Fourier spectral/Runge-Kutta-Gill scheme. This is a two-dimensional simulation. The initial field is given by a superposition of a simple shear flow, a periodic flow defined by

$$\overline{u}_1(x_2;0) = A \sin x_2 \tag{7}$$

and the $k_1 = 0$ component of random disturbances, whose spherically averaged energy spectrum is given by

$$E(k) = c\, k^4 \exp\left[-2k^2/k_p^2\right] \tag{8}$$

(Fig. 1). Here, c denotes the magnitude of the disturbances and k_p the peak wavenumber.

The shear rate S is set at unity. Several number of simulations are executed for different values of the Coriolis parameter f, the kinematic viscosity ν, the amplitude A of the periodic velocity (see (7)), and the amplitude u' and the peak wavenumber k_p of the initial disturbances. A rectangular computational domain of $0 \le x_2 < 2\pi$ and $0 \le x_3 < 32\pi$ is divided uniformly into 128×2048 grid points.

[3] Temporal evolution of mean velocity profile

3.1 Rossby-number dependence

First, we examine the Rossby-number dependence by changing the value of f (see Table I). The other parameters are fixed as $\nu = 2^{-8}$, $A = -1$, $u' = 1.25 \times 10^{-2}$, and $k_p = 8$. Figure 2 shows the temporal evolution of the mean velocity profile $\overline{u}_1(x_2;t)$ for (a) run2 (linearly stable system), (b) run3 (linearly neutral system), (c) run4 (linearly unstable system), and (d) run6 (linearly stable system).

Table II. Dependence on other parameters. Here, $\Delta\check{u}_1 = (\sqrt{3} - \pi/3)|A|$ and $\Delta x_2 = 2\pi/3$.

run	f	A	$u'/\lvert A\rvert$	k_p	ν	$Ra = f\Delta\check{u}_1\Delta{x_2}^3/\nu^2$
run2	1.5	-1	1.25×10^{-2}	8	3.91×10^{-3}	6.19×10^5
run2-lu'	1.5	-1	1.25×10^{-1}	8	3.91×10^{-3}	6.19×10^5
run2-su'	1.5	-1	1.25×10^{-3}	8	3.91×10^{-3}	6.19×10^5
run2-kp4	1.5	-1	1.25×10^{-2}	4	3.91×10^{-3}	6.19×10^5
run2-kp16	1.5	-1	1.25×10^{-2}	16	3.91×10^{-3}	6.19×10^5
run2-lowRa	1.5	-1	1.25×10^{-2}	8	1.10×10^{-2}	7.73×10^4
run2-hRa	1.5	-1	1.25×10^{-2}	8	1.38×10^{-3}	4.95×10^6
run2-A2	2.0	-2	1.25×10^{-2}	8	6.38×10^{-3}	6.19×10^5
run2-A05	1.25	-0.5	1.25×10^{-2}	8	2.52×10^{-3}	6.19×10^5

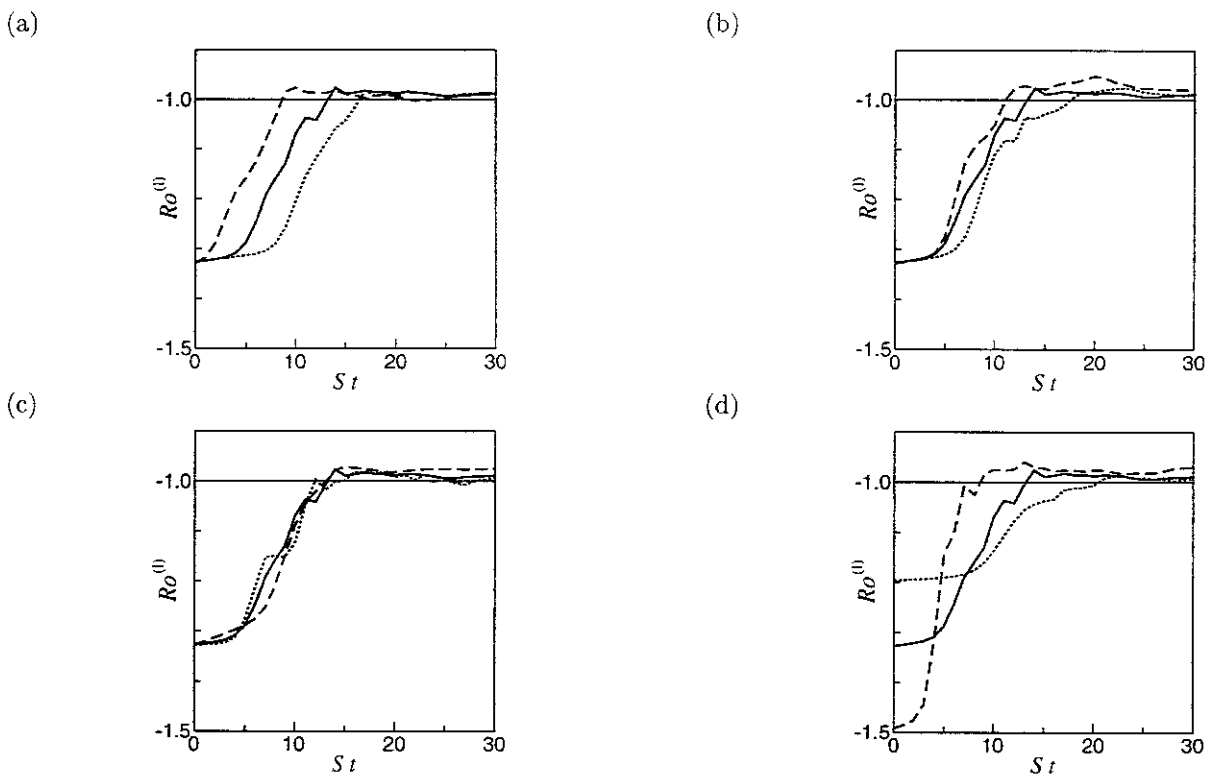

Fig. 3 Temporal evolution of local Rossby number at $x_2 = \pi$ for three values of (a) the amplitude u' (—; run2, – –; run2-lu', · · ·; run2-su') and (b) the peak wavenumber k_p (—; run2, – –; run2-kp4, · · ·; run2-kp16) of disturbances, (c) Rayleigh number Ra (—; run2, – –; run2-lowRa, · · ·; run2-hRa), and (d) the amplitude A of periodic velocity (—; run2, – –; run2-A2, · · ·; run2-A05).

In these figures the simple shear flow is subtracted to emphasize the variation in the x_2-direction. The flow is locally unstable where the gradient of the mean velocity, $\partial\overline{u}_1/\partial x_2$, is larger than that of the straight line of $Ro^{(l)}(x_2) = -1$. The initially unstable region ($Ro^{(l)}(x_2;0) < -1$) is denoted by a thick line on the right of each figure. The flow is locally unstable initially in the range of $2\pi/3 < x_2 < 4\pi/3$ for run2. The mean velocity profile changes in time in this unstable region and becomes linear by $St = 10$. The velocity gradient gradually decreases to approach a finite value, the associated absolute vorticity of which is nearly zero ($Ro^{(l)} \approx -1$). In contrast, the velocity profile has hardly changed around $x_2 = 0$ where the flow was linearly stable at the initial instant.

For run3 (neutral system) and run4 (unstable system) the mean velocity profile becomes linear in the locally unstable region as in the case of run2. However, the stable region is also broken up as opposed to the case of run2 and eventually the large-scale variation $\overline{u}_1(x_2;t)$ vanishes completely. Therefore, the mean velocity profile approaches back the simple shear flow and the stability characteristics is common throughout the whole region: it is neutral for run3 and unstable for run4. Since turbulence intensity increased monotonically in time for run4, the simulation was terminated at

$St = 12$ (the dash-dotted line represents the profile at the final stage).

Figure 2(d) shows that the mean velocity profile is almost invariant in time for run6. This is because the disturbances given at the initial instant decay and lose the ability to modify the mean velocity, since the whole region is linearly stable in this case. A slight change in the profile is mainly due to the viscous effect. The change in the mean velocity profile is not noticeable for run1 and run5 for the same reason (figures are omitted)

3.2 Dependences on other parameters

In order to clarify whether the results obtained for run2 are universal or not, several additional runs have been conducted for different values of the parameters. Here, the ratio $(|A|/(f-S))$ of vorticity of the periodic flow to the absolute mean vorticity is fixed to the value in run2, so that the flow is initially unstable in the range of $2\pi/3 < x_2 < 4\pi/3$. The strength of Coriolis force against viscosity may be measured by the 'Rayleigh number', $Ra = f\Delta\check{u}_1\Delta{x_2}^3/\nu^2$, which is an analogue of the Rayleigh number in a thermal convection (see §3.2 below). Here, Δx_2 $(= x_+ - x_-)$ is the width of the initial unstable region, $x_\pm$ being the upper and lower boundaries, and $\Delta\check{u}_1 = \overline{u}_1(x_+,0) - \overline{u}_1(x_-,0) - (f-S)\Delta x_2$ is the increment of the mean velocity across the unstable region relative to the neutral profile of $Ro^{(l)} = -1$ (see Fig. 5 below as well as Fig. 2(a)). Eight runs are carried out by changing A (with $|A|/(f-S)$ fixed), Ra, and the initial disturbances ($u'/|A|$ and k_p) separately (see Table II). The high-Rayleigh-number case (run2-hRa) is simulated with 256×2048 grid points.

In figure 3, we show the temporal evolution of the local Rossby number $Ro^{(l)}$ at $x_2 = \pi$ for three values of (a) the amplitude u' and (b) the peak wavenumber k_p of disturbances, (c) Rayleigh number Ra, and (d) the amplitude A of periodic velocity. There is the tendency in all cases that $Ro^{(l)}$ approaches close to -1, or the zero-absolute-vorticity state. The approach to -1 is closer for smaller scale (larger k_p) of disturbances, larger Rayleigh number, or smaller modulation of the mean shear (smaller A). This is consistent with theoretical results[13]. In summary, in an unstable region of a stable system the mean velocity profile is deformed into a linear one with nearly-zero absolute vorticity. This phenomenon seems very robust.

[4] Analogy with convective turbulence

When the turbulence field is uniform in the x_1-direction, an analogy holds between the rotating turbulent shear flow and thermally convective turbulence. This is not restricted to a linear limit as shown below Introducing new variables,

$$\check{u}_1 = u_1 - (f-S)x_2, \quad \check{p} = p + \frac{f(f-S)}{2}{x_2}^2. \tag{9}$$

we rewrite (2a) and (2b) as

$$\frac{\partial\check{u}_1}{\partial t} + \left(u_2\frac{\partial}{\partial x_2} + u_3\frac{\partial}{\partial x_3}\right)\check{u}_1 = \nu\left(\frac{\partial^2}{\partial {x_2}^2} + \frac{\partial^2}{\partial {x_3}^2}\right)\check{u}_1, \tag{10a}$$

$$\frac{\partial u_2}{\partial t} + \left(u_2\frac{\partial}{\partial x_2} + u_3\frac{\partial}{\partial x_3}\right)u_2 = -\frac{\partial\check{p}}{\partial x_2} - f\check{u}_1 + \nu\left(\frac{\partial^2}{\partial {x_2}^2} + \frac{\partial^2}{\partial {x_3}^2}\right)u_2. \tag{10b}$$

On the other hand, the thermal convection of a Boussinesq fluid is described by

$$\frac{\partial T}{\partial t} + \left(u_2\frac{\partial}{\partial x_2} + u_3\frac{\partial}{\partial x_3}\right)T = \kappa\left(\frac{\partial^2}{\partial {x_2}^2} + \frac{\partial^2}{\partial {x_3}^2}\right)T, \tag{11a}$$

$$\frac{\partial u_2}{\partial t} + \left(u_2\frac{\partial}{\partial x_2} + u_3\frac{\partial}{\partial x_3}\right)u_2 = -\frac{\partial p}{\partial x_2} + \alpha g T + \nu\left(\frac{\partial^2}{\partial {x_2}^2} + \frac{\partial^2}{\partial {x_3}^2}\right)u_2, \tag{11b}$$

where T, α, κ, and g are the temperature, the volume expansion coefficient, the thermal diffusivity coefficient, and the gravity constant, respectively. The gravity is assumed to point to the negative x_2-direction By comparing (10) and (11), especially buoyancy force $\alpha g T$ and Coriolis force $-f\check{u}_1$, we see that the temperature in the convective turbulence behaves in the same manner as the new variable $\check{u}_1$ in the rotating shear flow when $Pr = \nu/\kappa = 1$. A similar analogy was also pointed out in Veronis[14]. Note that the spanwise component of absolute vorticity is described by $\partial\check{u}_1/\partial x_2$, whereas that of fluctuating vorticity $\partial u_1/\partial x_2$.

It is seen in (10a) that if the flow is uniform in the x_1-direction, the variable $\check{u}_1$ is conserved under the advection. This is associated with supply of the (streamwise) momentum of $f\delta x_2$ by the Coriolis force[15,16] and of $-S\delta x_2$ by the simple shear flow (see the first term in the right-hand side of (2a)) when a fluid element moves in the x_2-direction by δx_2.

The above analogy enables us to interpret the results obtained in the preceding section as convective turbulence. The temporal evolution of the spatial distribution of $-\check{u}_1 = -u_1 + (f-S)x_2$ is shown in Fig. 4 for run2. The regions of $-\check{u}_1 \geq 0.2$ and $-\check{u}_1 \leq -0.2$ are respectively represented by red and blue which correspond to those of high and low temperature in convective turbulence when the gravity force is acting in the negative x_2-direction. Initially there is a region of 'low (or high) temperature' above (or below) the line $x_2 = \pi$ (Fig. 4(a)). In the unstable region, relatively small initial disturbances develop into plumes (Fig. 4(b)), extend to the vertical (x_2) direction, and develop into mushroom-like structures (Fig. 4(c)). They move around while mixing up

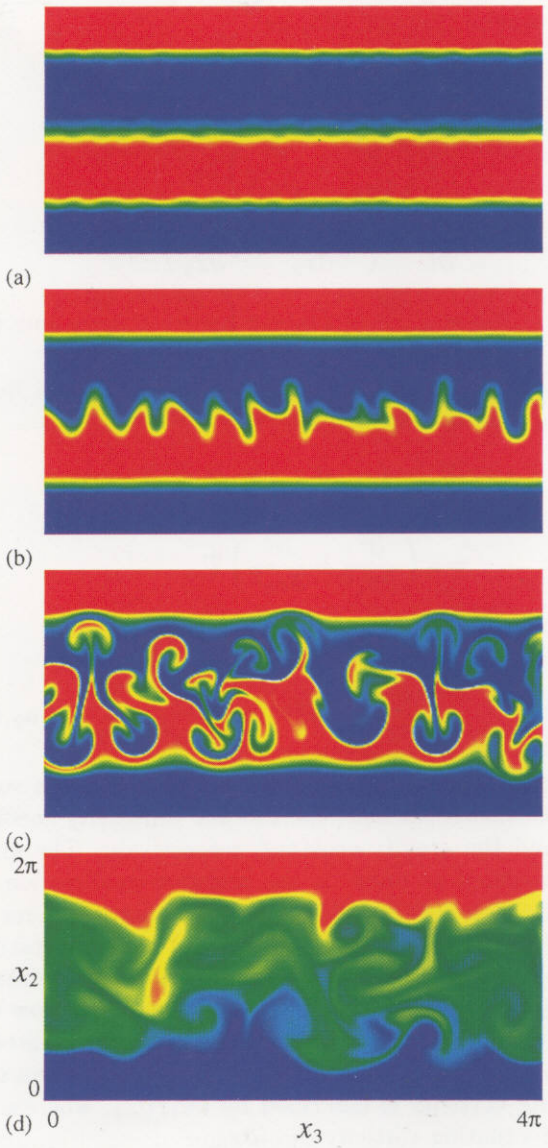

Fig. 4 Temporal evolution of the spatial distribution of $-\check{u}_1$ for run2. (a) $St = 0$, (b) 6, (c) 10, (d) 20. Red for $-\check{u}_1 \geq 0.2$ and blue for $-\check{u}_1 \leq 0.2$.

fluid elements of different temperature in the unstable region. The stable region is not influenced significantly by such disturbances since the vertical fluid motions are converted there to 'internal gravity waves'. Note that at least one locally stable region exists in a stable system but not necessarily in a neutral or an unstable system. Actually, the initially locally stable region is broken down by disturbances developed in adjacent unstable regions in these systems.

Finally, the fluid is sufficiently mixed in Fig. 4(d). At this time 'temperature' $-\check{u}_1$ is nearly uniform in this region (see Fig. 5). This means that the absolute vorticity $-\partial\check{u}_1/\partial x_2$ is nearly zero. In short, the state of zero absolute vorticity in a rotating turbulent shear flow corresponds to that of uniform temperature in convective turbulence. Bradshaw[9] mentioned an analogy between

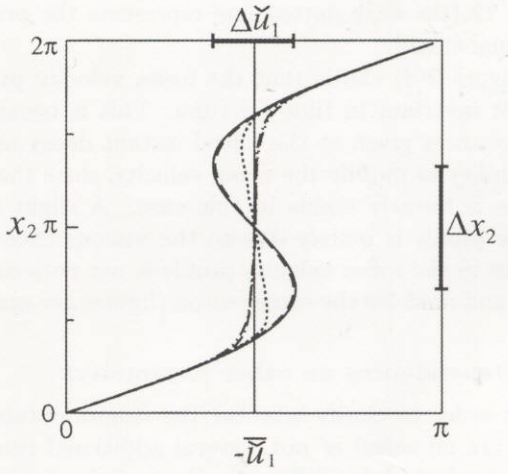

Fig. 5 Temporal evolution of $-\overline{\check{u}}_1$ for run2. — ; $St = 0$, – –; $St = 5$, · · · ; $St = 10$, – · – ; $St = 15$, – · · – ; $St = 20$, – · · · – ; $St = 25$. Δx_2 denotes the width of the initially unstable region. $\Delta\check{u}_1$ corresponds to the temperature difference ΔT in convective turbulence, so that we can define an analogue of the Rayleigh number as $\alpha g \Delta T \Delta {x_2}^3/\kappa\nu \rightarrow f\Delta\check{u}_1\Delta {x_2}^3/\nu^2$ when $Pr = 1$ (see §3.1.2).

the state of uniform temperature in free convection flow and that of zero absolute vorticity in an unstable rotating cylinder flow or a curved channel flow. In his paper, however, it is only stated that both cases correspond to a linearly neutral state of the flow. Equations (10) and (11), on the other hand, show that the analogy between a rotating shear flow and convective turbulence holds at nonlinear stage if the flow is uniform in the streamwise direction.

[5] Concluding remarks

We have investigated stability characteristics of a rotating simple shear flow modulated periodically in the shear direction. The temporal evolution and the final profile of the mean velocity perturbed initially by random disturbances are examined numerically, assuming that the velocity and pressure fields are uniform in the streamwise direction. It is found that in an unstable region of a stable system the mean velocity profile is deformed into a linear one with nearly-zero absolute vorticity, i.e., $Ro^{(l)} \approx -1$. An analogy holds at nonlinear level between rotating uniformly sheared turbulence and thermally convective turbulence if the flow field is uniform in the streamwise direction. Then, the region of nearly-zero absolute vorticity in the former corresponds to that of nearly-uniform temperature in the latter.

In the present study, we assume that the turbulence field is uniform in the streamwise direction. Actually, however, vortical structures in turbulent shear flows, such as longitudinal vortex tubes, are generally inclined from the streamwise direction. Since there are no such structures in convective turbulence, it is expected that

some differences appears between rotating shear turbulence and convection turbulence in a three-dimensional case.

In order to see the effects of this three-dimensionality of turbulence field, we have also conducted a fully three-dimensional simulation with the same parameters as run2. It is found that the linear mean profile appears in the three-dimensional case as well. However, the deviation of $Ro^{(l)}$ from -1 in this linear profile is more distinguished ($Ro^{(l)} \approx -0.9$) than that in the two-dimensional case. In their direct numerical simulation of rotating plane turbulent Couette flow, Bech & Andersson[8] also found the deviation ($Ro^{(l)} \approx -0.94$) in the linear mean velocity profile which appeared in the central region of the channel. The mechanism which causes such a deviation will be investigated in our further study.

References

[1] J.P. Johnston, R.M. Halleen, and D.K. Lezius, "Effects of spanwise rotation on the structure of two-dimensional fully developed turbulent channel flow," J. Fluid Mech. **56**, 533 (1972).

[2] K. Nakabayashi and O. Kitoh, "Low Reynolds number fully developed two-dimensional turbulent channel flow with system rotation," J. Fluid Mech. **315**, 1 (1996).

[3] R. Kristoffersen and H.I. Andersson, "Direct simulations of low-Reynolds-number turbulent flow in a rotating channel," J. Fluid Mech. **256**, 163 (1993).

[4] E. Lamballais, M. Lesieur, and O. Métais, "Influence d'une rotation d'entraînement sur les tourbillons cohérents dans un canal," C.R. Acad. Sci. Paris **323**, Série IIb, 95 (1996).

[5] M. Tanaka, "Vortical structures in homogeneously sheared turbulence subjected to background rotation," J. Phys. Soc. Japan **63**, 3914 (1994).

[6] M. Tanaka, S. Yanase, S. Kida, and G. Kawahara, "Vortical structures in rotating uniformly sheared turbulence," Flow, Turbulence and Combustion **60**, 301 (1998).

[7] O. Métais, C. Flores, S. Yanase, J.J. Riley and M. Lesieur, "Rotating free-shear flows. Part 2. Numerical simulation," J. Fluid Mech. **293**, 47 (1995).

[8] K.H. Bech and H.I. Andersson, "Turbulent plane Couette flow subject to strong system rotation," J. Fluid Mech. **347**, 289 (1997).

[9] P. Bradshaw, "The analogy between streamline curvature and buoyancy in turbulent shear flow," J. Fluid Mech. **36**, 177 (1969).

[10] T.J. Pedley, "On the stability of viscous flow in a rapidly rotating pipe," J. Fluid Mech. **35**, 97 (1969).

[11] S. Yanase, C. Flores, O. Métais, and J.J Riley, "Rotating free-shear flows. Part 1: Linear stability analysis," Phys. Fluids A **5**, 2725 (1993).

[12] S. Leblanc and C. Cambon, "On the three-dimensional instabilities of plane flows subjected to Coriolis force," Phys. Fluids **9**, 1307 (1997).

[13] F.H. Busse, "On Haward's upper bound for heat transport by turbulent convection," J. Fluid Mech. **37**, 457 (1969).

[14] G. Veronis, "The analogy between rotating and stratified fluids," Annu. Rev. Fluid Mech. **2**, 37 (1970).

[15] D.J. Tritton and P.A. Davies, "Instabilities in geophysical fluid dynamics," in *Hydrodynamic Instabilities and the Transition to Turbulence*, edited by H.L. Swinney and J.P. Gollub (Springer-Verlag, Berlin, 1981), p. 229.

[16] D.J. Tritton, "Stabilization and destabilization of turbulent shear flow in a rotating fluid," J. Fluid Mech. **241**, 503 (1992).

Recent Issues of NIFS Series

NIFS-560 S Sudo, K Kholopenkov, K Matsuoka, S Okamura, C. Takahashi, R Akiyama, A Fujisawa, K Ida, H Idei, H Iguchi, M Isobe, S Kado, K Kondo, S Kubo, H. Kuramoto, T Minami, S Morita, S Nishimura, M Osakabe M Sasao, B Peterson, K Tanaka, K Toi and Y Yoshimura,
Particle Transport Study with Tracer-Encapsulated Solid Pellet Injection, Oct 1998
(IAEA-CN-69/EXP1/18)

NIFS-561 A Fujisawa, H. Iguchi, S Lee, K. Tanaka, T. Minami, Y. Yoshimura, M Osakabe, K Matsuoka, S Okamura, H Idei, S Kubo, S Ohdachi, S. Morita, R. Akiyama, K. Toi, H Sanuki, K. Itoh, K. Ida, A. Shimizu, S Takagi, C. Takahashi, M Kojima, S Hidekuma, S. Nishimura, M Isobe, A Ejiri, N. Inoue, R Sakamoto, Y. Hamada and M Fujiwara,
Dynamic Behavior Associated with Electric Field Transitions in CHS Heliotron/Torsatron, Oct 1998
(IAEA-CN-69/EX5/1)

NIFS-562 S Yoshikawa,
Next Generation Toroidal Devices; Oct 1998

NIFS-563 Y Todo and T Sato,
Kinetic-Magnetohydrodynamic Simulation Study of Fast Ions and Toroidal Alfvén Eigenmodes; Oct. 1998
(IAEA-CN-69/THP2/22)

NIFS-564 T. Watari, T. Shimozuma, Y. Takeiri, R. Kumazawa, T. Mutoh, M. Sato, O Kaneko, K Ohkubo, S. Kubo, H Idei, Y Oka, M Osakabe, T. Seki, K. Tsumori, Y Yoshimura, R Akiyama, T Kawamoto, S Kobayashi, F Shimpo, Y Takita, E. Asano S Itoh, G Nomura, T. Ido, M. Hamabe, M Fujiwara, A. Iiyoshi, S. Morimoto, T Bigelow and Y P. Zhao,
Steady State Heating Technology Development for LHD, Oct. 1998
(IAEA-CN-69/FTP/21)

NIFS-565 A Sagara, K.Y. Watanabe, K Yamazaki, O. Motojima, M Fujiwara, O. Mitarai, S Imagawa, H Yamanishi, H. Chikaraishi, A. Kohyama, H. Matsui, T. Muroga, T Noda, N Ohyabu, T Satow, A A Shishkin, S Tanaka, T Terai and T Uda,
LHD-Type Compact Helical Reactors; Oct. 1998
(IAEA-CN-69/FTP/03(R)

NIFS-566 N Nakajima, J. Chen, K. Ichiguchi and M. Okamoto,
Global Mode Analysis of Ideal MHD Modes in L=2 Heliotron/Torsatron Systems; Oct. 1998
(IAEA-CN-69/THP1/08)

NIFS-567 K. Ida, M. Osakabe, K Tanaka, T. Minami, S. Nishimura, S Okamura, A. Fujisawa, Y Yoshimura, S. Kubo, R. Akiyama, D.S.Darrow, H. Idei, H. Iguchi, M. Isobe, S Kado, T. Kondo, S Lee, K. Matsuoka, S Morita, I Nomura, S Ohdachi, M Sasao, A Shimizu, K. Tumori, S. Takayama, M. Takechi, S. Takagi, C. Takahashi, K Toi and T Watari,
Transition from L Mode to High Ion Temperature Mode in CHS Heliotron/Torsatron Plasmas, Oct 1998
(IAEA-CN-69/EX2/2)

NIFS-568 S. Okamura, K Matsuoka, R. Akiyama, D.S. Darrow, A. Ejiri, A Fujisawa, M. Fujiwara, M Goto, K Ida H. Idei, H Iguchi, N. Inoue, M. Isobe, K. Itoh, S. Kado, K. Khlopenkov, T Kondo, S. Kubo, A. Lazaros, S. Lee, G Matsunaga, T. Minami, S. Morita, S Murakami, N Nakajima, N. Nikai, S. Nishimura, I Nomura, S. Ohdachi, K. Ohkuni, M Osakabe, R. Pavlichenko, B. Peterson, R Sakamoto, H Sanuki, M Sasao, A Shimizu, Y. Shirai, S Sudo, S. Takagi, C Takahashi, S. Takayama, M. Takechi, K. Tanaka K Toi, K Yamazaki, Y Yoshimura and T Watari,
Confinement Physics Study in a Small Low-Aspect-Ratio Helical Device CHS; Oct 1998
(IAEA-CN-69/OV4/5)

NIFS-569 M.M. Skoric, T Sato, A. Maluckov, M.S Jovanovic,
Micro- and Macro-scale Self-organization in a Dissipative Plasma, Oct 1998

NIFS-570 T Hayashi, N. Mizuguchi, T-H Watanabe, T. Sato and the Complexity Simulation Group,
Nonlinear Simulations of Internal Reconnection Event in Spherical Tokamak, Oct. 1998
(IAEA-CN-69/TH3/3)

NIFS-571 A Iiyoshi, A Komori, A. Ejiri, M. Emoto, H. Funaba, M. Goto, K Ida, H. Idei, S. Inagaki, S. Kado, O Kaneko, K. Kawahata, S Kubo, R Kumazawa, S. Masuzaki, T. Minami, J. Miyazawa, T Morisaki, S Morita, S. Murakami, S. Muto, T Muto, Y Nagayama, Y. Nakamura, H. Nakanishi, K. Narihara, K Nishimura, N. Noda, T Kobuchi, S Ohdachi, N Ohyabu, Y. Oka, M Osakabe, T. Ozaki, B.J. Peterson, A. Sagara, S. Sakakibara, R Sakamoto, H Sasao, M Sasao, K. Sato, M Sato, T. Seki, T Shimozuma, M. Shoji, H. Suzuki, Y. Takeiri, K Tanaka, K. Toi, T. Tokuzawa, K Tsumori, I. Yamada, H. Yamada, S Yamaguchi, M Yokoyama, K Y Watanabe, T. Watari, R. Akiyama, H. Chikaraishi, K. Haba, S Hamaguchi, S. Iima, S Imagawa, N. Inoue, K Iwamoto, S. Kitagawa, Y. Kubota, J Kodaira, R Maekawa, T. Mito, T. Nagasaka, A. Nishimura, Y. Takita, C. Takahashi, K. Takahata, K Yamauchi, H. Tamura, T Tsuzuki, S. Yamada, N Yanagi, H. Yonezu, Y Hamada, K Matsuoka, K. Murai, K. Ohkubo, I Ohtake, M. Okamoto, S Sato, T Satow, S Sudo, S. Tanahashi, K. Yamazaki, M Fujiwara and O Motojima,
An Overview of the Large Helical Device Project; Oct 1998
(IAEA-CN-69/OV1/4)

NIFS-572 M Fujiwara, H. Yamada, A. Ejiri, M Emoto, H. Funaba, M Goto, K. Ida, H. Idei, S Inagaki, S Kado, O. Kaneko, K Kawahata, A. Komori, S Kubo, R. Kumazawa, S. Masuzaki, T. Minami, J Miyazawa, T Morisaki, S. Morita, S. Murakami, S Muto, T. Muto, Y Nagayama, Y Nakamura, H. Nakanishi, K. Narihara, K. Nishimura, N Noda, T. Kobuchi, S Ohdachi, N Ohyabu, Y. Oka,

M. Osakabe, T. Ozaki, B. J. Peterson, A. Sagara, S. Sakakibara, R. Sakamoto, H. Sasao, M. Sasao, K. Sato, M. Sato, T. Seki, T Shimozuma, M. Shoji, H. Sazuki, Y. Takeiri, K Tanaka, K. Toi, T. Tokuzawa, K. Tsumori, I. Yamada, S Yamaguchi, M. Yokoyama, K.Y. Watanabe, T Watari, R. Akiyama, H. Chikaraishi, K. Haba, S Hamaguchi, M. Iima, S. Imagawa, N. Inoue, K. Iwamoto, S. Kitagawa, Y. Kubota, J. Kodaira, R. Maekawa, T. Mito. T. Nagasaka, A. Nishimura, Y. Takita, C. Takahashi, K. Takahata, K. Yamauchi, H. Tamura, T. Tsuzuki, S. Yamada, N. Yanagi, H. Yonezu, Y. Hamada, K. Matsuoka, K. Murai, K. Ohkubo, I. Ohtake, M. Okamoto, S. Sato, T. Satow, S. Sudo, S. Tanahashi, K. Yamazaki, O. Motojima and A. Iiyoshi,
Plasma Confinement Studies in LHD; Oct. 1998
(IAEA-CN-69/EX2/3)

NIFS-573 O. Motojima, K. Akaishi, H. Chikaraishi, H. Funaba, S. Hamaguchi, S. Imagawa, S Inagaki, N Inoue, A. Iwamoto, S Kitagawa, A. Komori, Y. Kubota, R. Maekawa, S. Masuzaki, T Mito, J. Miyazawa, T. Morisaki, T. Muroga, T Nagasaka, Y. Nakmura, A. Nishimura, K. Nishimura, N. Noda, N. Ohyabu, S. Sagara, S. Sakakibara, R. Sakamoto, S. Satoh, T Satow, M. Shoji, H. Suzuki, K. Takahata, H. Tamura, K. Watanabe, H. Yamada, S. Yamada, S. Yamaguchi, K. Yamazaki, N. Yanagi, T. Baba, H. Hayashi, M. Iima, T. Inoue, S. Kato, T. Kato, T. Kondo, S. Moriuchi, H. Ogawa, I. Ohtake, K. Ooba, H. Sekiguchi, N. Suzuki, S. Takami, Y Taniguchi, T. Tsuzuki, N. Yamamoto, K. Yasui, H. Yonezu, M. Fujiwara and A. Iiyoshi,
Progress Summary of LHD Engineering Design and Construction; Oct 1998
(IAEA-CN-69/FT2/1)

NIFS-574 K. Toi, M Takechi, S. Takagi, G Matsunaga, M. Isobe, T. Kondo, M Sasao, D.S Darrow, K. Ohkuni, S. Ohdachi, R. Akiyama A. Fujisawa, M. Gotoh, H. Idei, K. Ida, H. Iguchi, S. Kado, M. Kojima, S. Kubo, S. Lee, K. Matsuoka, T. Minami, S. Morita, N. Nikai, S. Nishimura, S. Okamura, M. Osakabe, A. Shimizu, Y. Shirai, C. Takahashi, K. Tanaka, T. Watari and Y. Yoshimura,
Global MHD Modes Excited by Energetic Ions in Heliotron/Torsatron Plasmas;Oct. 1998
(IAEA-CN-69/EXP1/19)

NIFS-575 Y Hamada, A. Nishizawa, Y Kawasumi, A. Fujisawa, M. Kojima, K. Narihara, K. Ida, A. Ejiri, S. Ohdachi, K. Kawahata, K. Toi, K. Sato, T Seki, H. Iguchi, K. Adachi, S. Hidekuma, S.Hirokura, K. Iwasaki, T Ido, R Kumazawa, H Kuramoto, T. Minami, I. Nomura, M. Sasao, K.N. Sato, T Tsuzuki, I Yamada and T Watari,
Potential Turbulence in Tokamak Plasmas;Oct 1998
(IAEA-CN-69/EXP2/14)

NIFS-576 S Murakami, U Gasparino, H. Idei, S. Kubo, H. Maassberg, N Marushchenko, N. Nakajima, M. Romé and M Okamoto,
5D Simulation Study of Suprathermal Electron Transport in Non-Axisymmetric Plasmas,Oct. 1998
(IAEA-CN-69/THP1/01)

NIFS-577 S. Fujiwara and T. Sato,
Molecular Dynamics Simulation of Structure Formation of Short Chain Molecules; Nov. 1998

NIFS-578 T Yamagishi,
Eigenfunctions for Vlasov Equation in Multi-species Plasmas Nov. 1998

NIFS-579 M. Tanaka, A. Yu Grosberg and T. Tanaka,
Molecular Dynamics of Strongly-Coupled Multichain Coulomb Polymers in Pure and Salt Aqueous Solutions;Nov. 1998

NIFS-580 J. Chen, N. Nakajima and M. Okamoto,
Global Mode Analysis of Ideal MHD Modes in a Heliotron/Torsatron System: I. Mercier-unstable Equilibria,Dec. 1998

NIFS-581 M. Tanaka, A. Yu Grosberg and T. Tanaka,
Comparison of Multichain Coulomb Polymers in Isolated and Periodic Systems: Molecular Dynamics Study; Jan. 1999

NIFS-582 V S. Chan and S. Murakami,
Self-Consistent Electric Field Effect on Electron Transport of ECH Plasmas; Feb 1999

NIFS-583 M. Yokoyama, N. Nakajima, M. Okamoto, Y. Nakamura and M. Wakatani,
Roles of Bumpy Field on Collisionless Particle Confinement in Helical-Axis Heliotrons;Feb. 1999

NIFS-584 T.-H. Watanabe, T. Hayashi, T. Sato, M. Yamada and H. Ji,
Modeling of Magnetic Island Formation in Magnetic Reconnection Experiment;Feb. 1999

NIFS-585 R. Kumazawa, T. Mutoh, T. Seki, F. Shinpo, G. Nomura, T. Ido, T. Watari, Jean-Marie Noterdaeme and Yangping Zhao,
Liquid Stub Tuner for Ion Cyclotron Heating;Mar 1999

NIFS-586 A. Sagara, M. Iima, S. Inagaki, N. Inoue, H. Suzuki, K. Tsuzuki, S. Masuzaki, J. Miyazawa, S. Morita, Y. Nakamura, N. Noda, B. Peterson, S. Sakakibara, T. Shimozuma, H. Yamada, K. Akaishi, H. Chikaraishi, H. Funaba, O. Kaneko, K. Kawahata, A. Komori, N. Ohyabu, O. Motojima, LHD Exp. Group 1, LHD Exp. Group 2,
Wall Conditioning at the Starting Phase of LHD;Mar. 1999

NIFS-587 T Nakamura and T. Yabe,
Cubic Interpolated Propagation Scheme for Solving the Hyper-Dimensional Vlasov-Poisson Equation in Phase Space, Mar 1999

NIFS-588 W X Wnag, N Nakajima, S Murakami and M Okamoto,
An Accurate δf Method for Neoclassical Transport Calculation, Mar 1999

NIFS-589 K. Kishida, K Araki, S Kishiba and K Suzuki,
Local or Nonlocal? Orthonormal Divergence-free Wavelet Analysis of Nonlinear Interactions in Turbulence, Mar. 1999

NIFS-590 K. Araki, K Suzuki, K Kishida and S Kishiba,
Multiresolution Approximation of the Vector Fields on T^3, Mar 1999

NIFS-591 K. Yamazaki, H. Yamada, K Y Watanabe, K Nishimura, S Yamaguchi, H Nakanishi, A Komori, H Suzuki, T Mito, H Chikaraishi, K. Murai, O Motojima and the LHD Group,
Overview of the Large Helical Device (LHD) Control System and Its First Operation, Apr 1999

NIFS-592 T. Takahashi and Y Nakao,
Thermonuclear Reactivity of D-T Fusion Plasma with Spin-Polarized Fuel, Apr 1999

NIFS-593 H. Sugama,
Damping of Toroidal Ion Temperature Gradient Modes, Apr. 1999

NIFS-594 Xiaodong Li ,
Analysis of Crowbar Action of High Voltage DC Power Supply in the LHD ICRF System; Apr 1999

NIFS-595 K Nishimura, R. Horiuchi and T Sato,
Drift-kink Instability Induced by Beam Ions in Field-reversed Configurations, Apr 1999

NIFS-596 Y. Suzuki, T-H. Watanabe, T. Sato and T. Hayashi,
Three-dimensional Simulation Study of Compact Toroid Plasmoid Injection into Magnetized Plasmas; Apr. 1999

NIFS-597 H Sanuki, K Itoh, M. Yokoyama, A Fujisawa, K. Ida, S. Toda, S.-I. Itoh, M. Yagi and A Fukuyama,
Possibility of Internal Transport Barrier Formation and Electric Field Bifurcation in LHD Plasma, May 1999

NIFS-598 S. Nakazawa, N. Nakajima, M. Okamoto and N. Ohyabu,
One Dimensional Simulation on Stability of Detached Plasma in a Tokamak Divertor; June 1999

NIFS-599 S. Murakami, N Nakajima, M. Okamoto and J Nhrenberg,
Effect of Energetic Ion Loss on ICRF Heating Efficiency and Energy Confinement Time in Heliotrons, June 1999

NIFS-600 R Horiuchi and T. Sato,
Three-Dimensional Particle Simulation of Plasma Instabilities and Collisionless Reconnection in a Current Sheet;; June 1999

NIFS-601 W. Wang, M. Okamoto, N. Nakajima and S Murakami,
Collisional Transport in a Plasma with Steep Gradients; June 1999

NIFS-602 T. Mutoh, R. Kumazawa, T. Saki, K Saito, F Simpo, G Nomura, T Watari, X. Jikang, G Cattanei, H Okada, K. Ohkubo, M Sato, S Kubo, T. Shimozuma, H Idei, Y Yoshimura, O Kaneko, Y. Takeiri, M Osakabe, Y Oka, K. Tsumori, A Komori, H Yamada, K Watanabe, S Sakakibara, M. Shoji, R Sakamoto, S Inagaki, J. Miyazawa, S Morita, K Tanaka, B.J. Peterson, S. Murakami, T Minami, S. Ohdachi, S Kado, K Narihara, H. Sasao, H. Suzuki, K Kawahata, N Ohyabu, Y Nakamura, H. Funaba, S. Masuzaki, S Muto, K Sato, T Morisaki, S Sudo, Y. Nagayama, T. Watanabe, M Sasao, K. Ida, N Noda, K. Yamazaki, K. Akaishi, A Sagara, K Nishimura, T. Ozaki, K Toi, O. Motojima, M. Fujiwara, A. Iiyoshi and LHD Exp Group 1 and 2,
First ICRF Heating Experiment in the Large Helical Device; July 1999

NIFS-603 P.C. de Vries, Y Nagayama, K Kawahata, S. Inagaki, H. Sasao and K Nagasaki,
Polarization of Electron Cyclotron Emission Spectra in LHD; July 1999

NIFS-604 W. Wang, N Nakajima, M Okamoto and S. Murakami,
δf Simulation of Ion Neoclassical Transport; July 1999

NIFS-605 T. Hayashi, N. Mizuguchi, T. Sato and the Complexity Simulation Group,
Numerical Simulation of Internal Reconnection Event in Spherical Tokamak, July 1999

NIFS-606 M. Okamoto, N. Nakajima and W. Wang,
On the Two Weighting Scheme for δf Collisional Transport Simulation; Aug. 1999

NIFS-607 O. Motojima, A.A. Shishkin, S. Inagaki, K. Y. Watanabe,
Possible Control Scenario of Radial Electric Field by Loss-Cone-Particle Injection into Helical Device; Aug 1999

NIFS-608 R. Tanaka, T. Nakamura and T. Yabe,
Constructing Exactly Conservative Scheme in Non-conservative Form; Aug. 1999

NIFS-609 H Sugama,
Gyrokinetic Field Theory; Aug 1999

NIFS-610 M. Takechi, G. Matsunaga, S. Takagi, K.Ohkuni, K. Toi, M. Osakabe, M Isobe, S. Okamura, K. Matsuoka, A. Fujisawa, H Iguchi, S. Lee, T. Minami, K. Tanaka, Y. Yoshimura and CHS Group,
Core Localized Toroidal Alfven Eigenmodes Destabilized By Energetic Ions in the CHS Heliotron/Torsatron; Sep. 1999

NIFS-611 K. Ichiguchi,
MHD Equilibrium and Stability in Heliotron Plasmas; Sep. 1999

NIFS-612 Y Sato, M. Yokoyama, M. Wakatani and V. D. Pusovitov,
Complete Suppression of Pfirsch-Schluter Current in a Toroidal l=3 Stellarator; Oct. 1999

NIFS-613 S. Wang, H. Sanuki and H Sugama,
Reduced Drift Kinetic Equation for Neoclassical Transport of Helical Plasmas in Ultra-low Collisionality Regime; Oct. 1999

NIFS-614 J. Miyazawa, H. Yamada, K. Yasui, S Kato, N., Fukumoto, M. Nagata and T. Uyama,
Design of Spheromak Injector Using Conical Accelerator for Large Helical Device; Nov. 1999

NIFS-615 M. Uchida, A. Fukuyama, K. Itoh, S.-I. Itoh and M. Yagi,
Analysis of Current Diffusive Ballooning Mode in Tokamaks; Dec. 1999

NIFS-616 M. Tanaka, A.Yu Grosberg and T. Tanaka,
Condensation and Swelling Behavior of Randomly Charged Multichain Polymers by Molecular Dynamics Simulations; Dec. 1999

NIFS-617 S. Goto and S. Kida,
Sparseness of Nonlinear Coupling; Dec. 1999

NIFS-618 M.M. Skoric, T. Sato, A. Maluckov and M.S. Jovanovic,
Complexity in Laser Plasma Instabilities Dec 1999

NIFS-619 T.-H. Watanabe, H. Sugama and T. Sato,
Non-dissipative Kinetic Simulation and Analytical Solution of Three-mode Equations of Ion Temperature Gradient Instability; Dec 1999

NIFS-620 Y. Oka, Y. Takeiri, Yu.I.Belchenko, M. Hamabe, O. Kaneko, K. Tsumori, M. Osakabe, E. Asano, T. Kawamoto, R. Akiyama,
Optimization of Cs Deposition in the 1/3 Scale Hydrogen Negative Ion Source for LHD-NBI System ;Dec 1999

NIFS-621 Yu.I. Belchenko, Y. Oka, O. Kaneko, Y. Takeiri, A. Krivenko, M. Osakabe, K. Tsumori, E. Asano, T. Kawamoto, R. Akiyama,
Recovery of Cesium in the Hydrogen Negative Ion Sources; Dec. 1999

NIFS-622 Y. Oka, O. Kaneko, K. Tsumori, Y. Takeiri, M. Osakabe, T. Kawamoto, E. Asano, and R. Akiyama,
H- Ion Source Using a Localized Virtual Magnetic Filter in the Plasma Electrode: Type I LV Magnetic Filter: Dec. 1999

NIFS-623 M. Tanaka, S Kida, S. Yanase and G. Kawahara,
Zero-absolute-vorticity State in a Rotating Turbulent Shear Flow; Jan. 2000